

Validation of 3D crack propagation in plain concrete. Part II: Computational modeling and predictions of the PCT3D test

T. Christian Gasser[†]

*Royal Institute of Technology (KTH), Department of Solid Mechanics,
Osquars backe 1, SE-100 44 Stockholm, Sweden
(Received April 30, 2006, Accepted February 5, 2007)*

Abstract. The discrete crack-concept is applied to study the 3D propagation of tensile-dominated failure in plain concrete. To this end the Partition of Unity Finite Element Method (PUFEM) is utilized and the strong discontinuity approach is followed. A consistent linearized implementation of the PUFEM is combined with a predictor-corrector algorithm to track the crack path, which leads to a robust numerical description of concrete cracking. The proposed concept is applied to study concrete failure during the PCT3D test and the predicted numerical results are compared to experimental data. The proposed numerical concept provides a clear interface for constitutive models and allows an investigation of their impact on concrete cracking under 3D conditions, which is of significant scientific interests to interpret results from 3D experiments.

Keywords: concrete cracking; partition of unity finite element method; strong discontinuity; 3D crack-tracking; PCT3D test.

1. Introduction

The study of failure propagation in concrete structures is of major engineering importance and under extensive scientific interest during the past three decades. Concrete failure causes a sizeable nonlinear zone at the fracture front, and hence, classical linear fracture mechanics of sharp cracks is an inadequate concept to be used (Kesler, *et al.* 1972).

Tensile-dominated failure of plain concrete involves progressive micro-cracking, debonding and other complex irreversible processes of internal damage. The associated strain-softening can coalesce into a geometrical discontinuity, where damage and other inelastic effects are limited to zones of small volume, while the main portion of the material deforms purely elastic. The discrete crack-concept is the approach that reflects this phenomena closest, and hence, it gained wide popularity for numerical simulations of concrete fracture. Plasticity effects are negligible of tensile-dominated failure, and under that circumstances, concrete can be considered as a quasi-brittle material (Bažant 2002). However, the pronounced strain softening of concrete failure let a description within polar (local) continuum mechanics fail (Bažant and Pijaudier-Cabot 1988), and motivates the application of advanced continuum mechanical theories.

Constitutive modeling of concrete failure is an active scientific field and numerous constitutive models for concrete have been proposed in the past. Failure models of concrete are based on

[†] E-mail: tg@half.kth.se <http://www.half.kth.se/~tg/>

plasticity theories, fracture theories (fixed crack, rotating crack and multi-non-orthogonal fixed crack methods), damage theories and formulations which couple these approaches, see (Jefferson 2003a, b, Feist and Kerber 2004). In particular, the comparative study of 3D constitutive models for concrete (Pivonka, *et al.* 2004) highlights diverging results achieved with different models. In addition, only a limited number of well documented 3D fracture tests (the torsional test (Brokenshire 1996) is one of the rare examples) are available in the literature to validate 3D constitutive models for concrete.

The present work aims to model 3D crack propagation in plain concrete under mixed mode situations, where the underlying continuum mechanical framework is introduced in Section 2.1. It is assumed that the cohesive properties of the material dominate over the frictional one, and hence, fracture parameters of the opening mode (mode I) quantify concrete cracking. Herein, the model proposed in Gasser and Holzapfel (2005) is utilized, and its constitutive assumption are discussed in Section 2.1.3. It needs to be emphasized, that cohesive modeling is a well-established field, and various cohesive constitutive formulations have been presented in the past, see, amongst many others, (Needleman 1987, 1990, Tvergaard and Hutchinson 1992, Ortiz and Pandolfi 1999). In that context the reader is referred to the seminal work (Bažant 2002), where limitations of cohesive models in general are discussed.

The **Partition of Unity Finite Element Method** (PUFEM) (Melenk and Babuška 1996) is the numerical concept chosen to describe 3D crack propagation in plain concrete; it is briefly reviewed in Section 2.2. PUFEM provides an effective and robust numerical frame (Wells, *et al.* 2002, Gasser and Holzapfel 2005) with several advantages over traditional smeared and discrete approaches, see (Jirásek 2000, Jirásek and Belytschko 2002, de Borst 2001). In particular, the applied numerical concept provides a clear interface to integrate cohesive models and its numerical implementation is discussed in detail in Section 2.2.1.

A critical task to apply PUFEM is the geometrical representation of the crack surface and tracking its propagation during concrete failure. To this end different numerical techniques are proposed, where a classification in *local* (Moës, *et al.* 2002), *global* (Oliver, *et al.* 2004) and *partial domain* (Feist and Hofstetter 2007) crack-tracking algorithms are proposed in the literature. Within this work, the recently proposed local crack-tracking algorithm (Gasser and Holzapfel 2005) is adopted, which is based on a predictor-corrector schema to track non-planar 3D cracks; it is briefly reviewed in Section 2.3.

The underlying work aims to validate the proposed numerical concept of concrete failure, i.e., PUFEM combined with the predictor-corrector scheme to track the crack path. To this end the PCT3D test, an experiment to investigate 3D cracking of plane concrete performed at the *University of Innsbruck, Austria*, is numerically investigated. A comprehensive description of the PCT3D test and its experimental findings are given in the companion paper (Feist and Hofstetter 2007), and in Section 3 herein, this data is compared to computationally predicted results. In particular, the **load-Crack Mouth Opening Displacement (CMOD)** response, the developed 3D crack formation and the evolution of the strain field are investigated.

2. Crack propagation model

Failure of concrete is accompanied by pronounced strain-softening, and hence, its description within standard polar continuum mechanics fails. The energy at failure is incorrectly predicted to zero (Bažant and Pijaudier-Cabot 1988) and this physically meaningless solution is approximated by the numerical schema applied, which *a priori* leads to pathologically mesh sensitivity of the numerical

solution. Advanced theories, e.g., non-local damage models, *Cosserat* models, rate-dependent models, gradient-enhanced models can overcome this lack of the standard continuum and define a well posed **Boundary Value Problem** (BVP). In this work the discrete crack-concept is followed and the underlying continuum mechanical basis and its numerical implementation is discussed in the following.

2.1. Continuum mechanical basis

2.1.1. Kinematics

It is assumed that Ω_0 denotes the reference configuration of a body with an embedded strong discontinuity $\partial\Omega_{0d}$, which separates the body into the sub-domains Ω_{0+} and Ω_{0-} , respectively¹. The motion $\chi(\mathbf{X})$ maps Ω_{0+} and Ω_{0-} into their current configurations, i.e., Ω_+ and Ω_- , where \mathbf{X} denotes the referential position of a material point. Moreover, the kinematics of the separation are captured by a discontinuity in the displacement field, i.e., $\mathbf{u}(\mathbf{X}) = \mathbf{u}_c(\mathbf{X}) + \mathcal{H}(\mathbf{X})\mathbf{u}_e(\mathbf{X})$, where \mathcal{H} denotes the *Heaviside* function with the value 0 for $\mathbf{X} \in \Omega_{0-}$ and 1 for $\mathbf{X} \in \Omega_{0+}$. Note that the introduced additive decomposition of \mathbf{u} is based on the introduction of the smooth fields \mathbf{u}_c and \mathbf{u}_e , which characterize the compatible and the enhanced displacements, respectively.

Consequently, the deformation gradient reads

$$\mathbf{F}(\mathbf{X}) = \mathbf{I} + \text{Grad } \mathbf{u}_c(\mathbf{X}) + \mathcal{H} \text{Grad } \mathbf{u}_e(\mathbf{X}) + \delta_d(\mathbf{X})\mathbf{u}_e(\mathbf{X}) \otimes \mathbf{N}(\mathbf{X}_d), \quad (1)$$

where the property $\text{Grad } \mathcal{H}(\mathbf{X}) = \delta_d \mathbf{N}(\mathbf{X}_d)$ of the *Heaviside* function is utilized and δ_d denotes the *Dirac-delta* functional with the value 0 for $\mathbf{X} \notin \partial\Omega_{0d}$ and ∞ for $\mathbf{X} \in \partial\Omega_{0d}$. In addition, the material gradient operator is denoted by $\text{Grad}(\bullet) = \partial(\bullet)/\partial\mathbf{X}$, and the unit normal vector $\mathbf{N}(\mathbf{X}_d)$ defines the orientation of the discontinuity at an arbitrary (referential) point $\mathbf{X}_d \in \partial\Omega_{0d}$.

For reasons that become clear in the following section, it is convenient to consider separate deformation gradients for the two sub-domains, i.e., a compatible deformation gradient $\mathbf{F}_c = \mathbf{I} + \text{Grad} \mathbf{u}_c$ (with $\mathbf{F}_c = J_c > 0$), which maps Ω_{0-} into Ω_- , and an enhanced deformation gradient $\mathbf{F}_e = \mathbf{I} + \text{Grad} \mathbf{u}_c + \text{Grad} \mathbf{u}_e$ (with $\det \mathbf{F}_e = J_e > 0$), which maps Ω_{0+} into Ω_+ .

A geometrical exact formulation is followed, and hence, a *fictitious discontinuity* $\partial\Omega_d$, i.e., the bijection of $\partial\Omega_{0d}$ to the current configuration, needs to be introduced. To this end the works (Varias, *et al.* 1990, Wells, *et al.* 2002) are followed, and $\partial\Omega_d$ is placed in the middle between the two physical crack surfaces, such that, $\partial\Omega_d$ is defined by the *push forward* of $\partial\Omega_{0d}$ associated with the average deformation gradient $\mathbf{F}_d(\mathbf{X}_d) = \mathbf{I} + \text{Grad } \mathbf{u}_c + \mathbf{u}_e \otimes \mathbf{N}/2$ (with $\det \mathbf{F}_d = J_d > 0$). Consequently, the mapping transforms the referential point $\mathbf{X}_d \in \partial\Omega_{0d}$ into the spatial point $\mathbf{x}_d = \mathbf{F}_d \mathbf{X}_d$ with $\mathbf{x}_d \in \partial\Omega_d$. The related unit normal vector $\mathbf{n} = \mathbf{N} \mathbf{F}_d^{-1} / |\mathbf{N} \mathbf{F}_d^{-1}|$ onto the fictitious discontinuity is obtained by a weighted *push-forward* operation of the covariant vector \mathbf{N} . Note that, although small strain characterizes the bulk material of tensile-dominated concrete failure, large rotations may be present, which motivates the application of a geometrically exact formulation.

2.1.2. Variational formulation

This section is included in order to briefly discuss the consequences of the introduced kinematics on a single-field variational approach; detailed derivations are given in Wells, *et al.* (2002), Gasser and Holzapfel (2005). For simplicity, inertia effects are neglect and dead loading is assumed, such

¹For simplicity a single embedded discontinuity is considered, although the proposed concept can be applied to multiple non-interacting discontinuities as well.

that $\int_{\Omega_0} \text{Grad} \delta \mathbf{u} : \mathbf{P}(\mathbf{F}) dV - \delta \Pi^{\text{ext}}(\delta \mathbf{u}) = 0$ holds (Ogden 1997, Holzapfel 2000), where $\mathbf{P}(\mathbf{F})$ and $\delta \mathbf{u}$ denote the first Piola-Kirchhoff stress tensor and the admissible variation of the displacement field, respectively. According to the introduced additive split of the displacement field \mathbf{u} , its admissible variation is defined by $\delta \mathbf{u} = \delta \mathbf{u}_c + \mathcal{H} \delta \mathbf{u}_e$. Consequently, straight forward algebraic manipulation and a *push-forward* of the above introduced single-field variational principle gives the two spatial variational statements (Gasser and Holzapfel 2005).

$$\left. \begin{aligned} \int_{\Omega_-} \text{sym}(\text{grad}_c \delta \mathbf{u}_c) : \boldsymbol{\sigma}_c dv + \int_{\Omega_+} \text{sym}(\text{grad}_e \delta \mathbf{u}_e) : \boldsymbol{\sigma}_e dv - \delta \Pi_c^{\text{ext}}(\delta \mathbf{u}_c) = 0, \\ \int_{\Omega_+} \text{sym}(\text{grad}_e \delta \mathbf{u}_e) : \boldsymbol{\sigma}_e dv + \int_{\partial \Omega_d} \mathbf{t} \cdot \delta \mathbf{u}_e ds - \delta \Pi_e^{\text{ext}}(\delta \mathbf{u}_e) = 0, \end{aligned} \right\} \quad (2)$$

where dv is the infinitesimal volume element defined in the current configuration and ds is the infinitesimal surface element defined on the discontinuity $\partial \Omega_d$. Moreover, $\boldsymbol{\sigma}_c = J_c^{-1} \mathbf{P}(\mathbf{F}_c) \mathbf{F}_c^T$ and $\boldsymbol{\sigma}_e = J_e^{-1} \mathbf{P}(\mathbf{F}_e) \mathbf{F}_e^T$ denote Cauchy stress tensors and \mathbf{t} characterizes the Cauchy traction vector acting on the fictitious discontinuity $\partial \Omega_d$. Contributions due to external loading are summarized in terms of the virtual external potential energies $\delta \Pi_c^{\text{ext}}$ and $\delta \Pi_e^{\text{ext}}$, which refer to the domains Ω_{0-} and Ω_{0+} , respectively. The spatial gradients in Eq. (2) are defined according to $\text{grad}_c(\bullet) = \text{Grad}(\bullet) \mathbf{F}_c^{-1}$, $\text{grad}_e(\bullet) = \text{Grad}(\bullet) \mathbf{F}_e^{-1}$ and the operator $\text{sym}(\bullet) = [(\bullet) + (\bullet)^T]/2$ furnishes the symmetric part of (\bullet) .

2.1.3. Constitutive formulations

Constitutive formulations play a fundamental role of reliable numerical simulations of concrete failure, and under 3D loading conditions no constitutive model enjoys wide acceptance. Models known from the literature can predict significantly different results under 3D loading conditions, which has been demonstrated, for the double-edge-notched specimen (DENS) applied to tensile and shear loadings (Pivonka, *et al.* 2004).

Tensile-dominated failure of concrete causes zones of small volume, where accumulation of damage and other inelastic effects are present, while the main portion of the material deforms purely elastic. Consequently, a natural modeling assumption is the coupling of an elastic bulk material with an inelastic cohesive zone. This is a simple way to capture the physical phenomena, and it avoids the introduction of damage-based softening in the bulk material. However, the proposed approach requires two constitutive models, i.e., (i) bulk (continuous) and (ii) cohesive (discontinuous) material models, characterizing the elastic and inelastic properties of concrete. Note that, theoretically spoken, every continuum constitutive model linked to strong discontinuity kinematics defines a discrete model in a consistent way (Oliver 2000, Oliver, *et al.* 2002). Nevertheless, the classical approach is followed herein, where the cohesive material model is assumed to be independent from the bulk material. From the practical point of view this decoupling of the continuous and discontinuous constitutive models gives more flexibility in fitting experimental data.

Bulk material response. It is assumed that the concrete's bulk (or continuous) response is captured by a neoHookean material according to the strain-energy function $\Psi(\mathbf{C})$ in the additive decomposed form (Holzapfel 2000)

$$\Psi(\mathbf{C}) = \kappa (\ln J)^2 + \frac{\mu}{2} (\bar{I}_1 - 3), \quad (3)$$

where κ and μ denote the bulk and shear moduli, respectively. Here, $\bar{I}_1 = \text{tr}(\bar{\mathbf{C}})$ is the first invariant of the modified right Cauchy-Green tensor $\bar{\mathbf{C}} = J^{-2/3}\mathbf{C}$, where $\mathbf{C} = \mathbf{F}^T\mathbf{F}$ and classical derivations, e.g., (Holzapfel 2000) lead to the Cauchy stress $\boldsymbol{\sigma} = 2J^{-1}\mathbf{b}\partial\Psi/\partial\mathbf{b}$ and the associated spatial elasticity tensor $\mathbf{C} = 4J^{-1}\mathbf{b}(\partial^2\Psi/\partial\mathbf{b}\partial\mathbf{b})\mathbf{b}$, where $\mathbf{b} = \mathbf{F}\mathbf{F}^T$ denotes the left Cauchy-Green tensor.

Cohesive material response. The cohesive (or discontinuous) material property is determined by a number of material-dependent mechanisms such as cohesion at the atomistic scale, bridging ligaments, interlocking of grains and other inelastic phenomena. In order to capture these mechanisms in a phenomenological sense, the existence of a cohesive potential with respect to the reference configuration $\partial\Omega_{0d}$ of the discontinuity is postulated and the recently proposed transversely isotropic model (Gasser and Holzapfel 2005) is adopted. The model is based on the theory of invariants (Spencer 1984) and assumes a cohesive potential of the form $\psi^{\text{coh}} = \psi^{\text{coh}}(\mathbf{u}_e \otimes \mathbf{u}_e, \mathbf{n} \otimes \mathbf{n}, \delta)$, where $\mathbf{u}_e(\mathbf{X}_d)$ denotes the gap displacement, i.e., the enhanced displacement at the discontinuity. In addition, transverse isotropy and the state of damage are defined by the structural tensor $\mathbf{n} \otimes \mathbf{n}$ and a single scalar internal variable $\delta \in [0, \infty]$, respectively. Following (Spencer 1984), the cohesive potential can be expressed according to $\psi^{\text{coh}} = \psi^{\text{coh}}(i_1, i_2, i_3, i_4, i_5, \delta)$, where i_1, \dots, i_5 are invariants depending on the symmetric tensors $\mathbf{u}_e \otimes \mathbf{u}_e$, and $\mathbf{n} \otimes \mathbf{n}$. Within this paper the isotropic particularization

$$\psi^{\text{coh}}(i_1, \delta) = \frac{t_0}{2\delta} \exp(-a\delta^b) i_1 \quad (4)$$

is applied, where $i_1 = \mathbf{u}_e \cdot \mathbf{u}_e$ denotes the first invariant of $\mathbf{u}_e \otimes \mathbf{u}_e$. Here t_0 denotes the cohesive tensile strength of concrete and the non-negative parameters a and b aim to capture its softening response under mode I failure. The cohesive potential (4) is able to capture the tensile failure properties of concrete, as illustrated in Gasser and Holzapfel (2005), where the set (t_0, a, b) has been determined by least square optimization of experimental data given in Reinhardt, *et al.* (1986).

In order to complete the cohesive description a damage surface $\phi^{\text{coh}}(\mathbf{u}_e, \delta) = |\mathbf{u}_e| - \delta = 0$ in the gap displacement space is defined, and $\delta = |\bar{\mathbf{u}}_e|$ models the evolution of the internal (damage) variable δ . Based on the procedure by Coleman and Noll (Coleman and Noll 1963) the referential cohesive traction reads, $\mathbf{T}^{\text{coh}} = \partial\psi^{\text{coh}}/\partial\mathbf{u}_e$ and for a subsequent finite element implementation, it is convenient to introduce $\mathbf{C}_{\mathbf{u}_e}^{\text{coh}} = \partial\mathbf{T}^{\text{coh}}/\partial\mathbf{u}_e + (\partial\mathbf{T}^{\text{coh}}/\partial\delta)(\partial\delta/\partial\mathbf{u}_e)$, $\mathbf{C}_{\mathbf{n}}^{\text{coh}} = \partial\mathbf{T}^{\text{coh}}/\partial\mathbf{n}$, which characterize stiffness measures with respect to changes of the gap displacement and the orientation of the discontinuity.

Failure criterion. It is well known that material stability is violated in the Mandel sense (Mandel 1966) if the acoustic tensor \mathbf{Q} becomes singular, and hence, acceleration waves cannot propagate through the solid at finite speed at every direction. This is a necessary but not sufficient condition for strain localization, and several other conditions are discussed in the literature, such as positive definiteness/singularity of the constitutive operator, strong ellipticity, flutter etc., see, e.g., Bigoni and Zaccaria (1994). The concept of localization is well-established and extensively documented in the literature, see, e.g., Rudnicki and Rice (1975), however, its numerical representation may be associated with high computational costs for the general 3D case.

For plain concrete, computationally less expensive failure criteria are available as well, in particular, the Rankine criterion seems to provide sufficient accuracy. Here it is assumed that failure initializes if the maximum principal Cauchy stress σ_{max} reaches the concrete's tensile strength t_0 and the orientation \mathbf{n} of the failure is determined by the direction of the maximum principal stress.

It is known that the coupling of the local *Rankine* criterion with a local crack-tracking algorithm can lead to a scattered crack path. Consequently, several techniques are known in the literature to avoid this kind of instability, e.g., averaging the orientation of the discontinuity (Wells and Sluys 2001) or non-local evaluation of the *Rankine* criterion (Gasser and Holzapfel 2005). Note that averaging the stress field can cause non-physical crack initialization (Simone, *et al.* 2004), especially at stress (strain) singularities. Nevertheless, the non-local *Rankine* criterion, which requires the solution of the eigenvalue problem

$$(\bar{\boldsymbol{\sigma}}(\mathbf{x}) - \lambda_i \mathbf{I}) \mathbf{v}_i = \mathbf{0}, \quad \text{no summation over } i \quad (5)$$

at a spatial point \mathbf{x} , is utilized within this work. Here λ_i and \mathbf{v}_i are the eigenvalues and eigenvectors and the underlying stress $\bar{\boldsymbol{\sigma}}$ is averaged within the vicinity of \mathbf{x} . In particular, $\bar{\boldsymbol{\sigma}}(\mathbf{x}) = \frac{\int_{\Omega_0(\mathbf{x})} \boldsymbol{\sigma}(\mathbf{x}) dV}{\int_{\Omega_0(\mathbf{x})} dV}$ is proposed, where $\Omega_0(\mathbf{X})$ denotes a spherical region with center at $\mathbf{X} = \mathbf{F}^{-1} \mathbf{x}$ and radius R .

Finally, it is worth noting that a non-local evaluation of the *Rankine* criterion is not sufficient to avoid the evolution of an unreasonable cracks in 3D, which is explained (to some extent) in Section 2.3.

2.2. PUFEM

The variational statements (2) are numerically represented by means of the PUFEM (Melenk and Babuška 1996), where the standard (polynomial) interpolation functions are enriched by the *Heaviside* function \mathcal{H} to achieve good local approximation properties for the underlying problem. In particular, the displacement field \mathbf{u} is interpolated by²

$$\mathbf{u} = \sum_{i=1}^{n_{\text{elem}}} N^I \mathbf{u}_{Ic} + \mathcal{H} \sum_{i=1}^{n_{\text{elem}}} N^I \mathbf{u}_{Ie}, \quad (6)$$

where N^I are the standard (polynomial) interpolation functions. Here I is an index running between 1 and the total number of element nodes n_{elem} . Interpolation (6) falls into the class of the PUFEM, where regular and enhanced nodal displacements (degrees of freedom) are denoted by \mathbf{u}_{Ic} and \mathbf{u}_{Ie} , respectively. Elaboration on basis of the interpolation (6) and the two spatial variational statements (2) leads to the linearized algebraic set

$$\begin{bmatrix} \mathbf{K}_{\mathbf{u}_c \mathbf{u}_c} & \mathbf{K}_{\mathbf{u}_c \mathbf{u}_e} \\ \mathbf{K}_{\mathbf{u}_e \mathbf{u}_c} & \mathbf{K}_{\mathbf{u}_e \mathbf{u}_e} \end{bmatrix}_{i-1}^e \begin{bmatrix} \Delta \mathbf{u}_c \\ \Delta \mathbf{u}_e \end{bmatrix}_i^e = \begin{bmatrix} \mathbf{f}_{\mathbf{u}_c}^{\text{ext}} \\ \mathbf{f}_{\mathbf{u}_c}^{\text{int}} \end{bmatrix}_{i-1}^e - \begin{bmatrix} \mathbf{f}_{\mathbf{u}_c}^{\text{int}} \\ \mathbf{f}_{\mathbf{u}_e}^{\text{int}} \end{bmatrix}_{i-1}^e \quad (7)$$

of equations for a particular finite element e (Gasser and Holzapfel 2006). Here $i, i-1$ and $\Delta \mathbf{u}_c, \Delta \mathbf{u}_e$ denote the iteration steps associated with a global iteration procedure, and the increments of the regular and enhanced nodal displacements, respectively.

In Eq. (7) the force vectors $\mathbf{f}_{\mathbf{u}_c}^{\text{ext}}, \mathbf{f}_{\mathbf{u}_e}^{\text{ext}}$ and $\mathbf{f}_{\mathbf{u}_c}^{\text{int}}, \mathbf{f}_{\mathbf{u}_e}^{\text{int}}$ denote nodal force due to external and internal loadings, whereas the subscripts $(\bullet)_{\mathbf{u}_c}$ and $(\bullet)_{\mathbf{u}_e}$ denote their association with compatible and enhanced degrees of freedom, respectively. The stiffness matrices $\mathbf{K}_{\mathbf{u}_c \mathbf{u}_c}, \mathbf{K}_{\mathbf{u}_c \mathbf{u}_e}, \mathbf{K}_{\mathbf{u}_e \mathbf{u}_c}, \mathbf{K}_{\mathbf{u}_e \mathbf{u}_e}$ are defined due to a consistent linearization of the internal loading vectors with respect to the compatible and enhanced displacements, details are given in Gasser and Holzapfel (2005). It is worth noting that, in general, the cohesive traction contributes to $\mathbf{f}_{\mathbf{u}_c}^{\text{int}}, \mathbf{K}_{\mathbf{u}_c \mathbf{u}_c}$ and $\mathbf{K}_{\mathbf{u}_e \mathbf{u}_e}$ (Gasser and Holzapfel 2003a, 2005) and the element stiffness matrix becomes non-symmetric, such that,

²Characters indicated by underlines denote the matrix notation of the associated tensor or vector. For example, $\underline{\mathbf{u}}$ is the matrix representation of vector \mathbf{u} .

appropriate solution strategies are required. However, for the considered numerical example given in Section 3, a symmetric solver has been applied and the computation has shown (about) quadratic convergence, which indicates negligible asymmetry of the element stiffness matrix in this case.

2.2.1. Numerical implementation of the cohesive zone model

The cohesive model Eq. (4) is implemented in a separate material routine, where the gap displacement $\mathbf{u}_e(\mathbf{x}_d^l)$ and the spatial normal $\mathbf{n}(\mathbf{x}_d^l)$ of the current iteration step and the damage variable $\delta_n(\mathbf{x}_d^l)$ of last solution step are input data. Here \mathbf{x}_d^l denotes the l -th integration point at the discontinuity and the discrete material routine computes the traction and the stiffness quantities, as it is required to arrange system, Eq. (7) (Gasser and Holzzapfel 2005). In addition, the proposed numerical approach aims to avoid penetration of the subbodies Ω_+ and Ω_- under compressive loading of the cohesive zone. Hence, in case that $u_n = \mathbf{u}_e(\mathbf{x}_d^l) \cdot \mathbf{n}(\mathbf{x}_d^l) > 0$ holds, a penalty constraint is added to the cohesive potential, which is similar to penalty constraint formulations in contact mechanics (Wriggers 2002). Within this work the quadratic penalty potential $\psi_{\text{pen}}(\mathbf{u}_e, \mathbf{n}) = k(\mathbf{u}_e, \mathbf{n})^2/2$ is applied, where k denotes the problem specific penalty parameter.

Consequently, for a particular state of damage δ_n , the total surface potential $\psi(\mathbf{u}_e, \mathbf{n}, \delta_n)$, i.e., cohesive and penalty contributions read

$$\psi(\mathbf{u}_e, \mathbf{n}, \delta_n) = \frac{c_n}{2}(\mathbf{u} \cdot \mathbf{u}) + \frac{k}{2} \langle \mathbf{u}_e, \mathbf{n} \rangle^2, \quad c_n = t_n / \delta_n, \quad (8)$$

where $\langle (\bullet) \rangle = [(\bullet) + |(\bullet)|]/2$ denotes the *Macaulay* bracket. Here $t_n = t_0 \exp(-a\delta_n^b)$ and c_n denote the elastic limit and a scalar stiffness measure of the cohesive zone at the state of damage δ_n . An illustration of the cohesive law and the introduced quantities δ_n , t_n and c_n is given in Fig. 1, where the gray and black lines denote elastic and damage loading branches, respectively.

In order to provide the solution for the current global iteration step, the system (7) is solved, which gives the enhanced displacement \mathbf{u}_e , and hence, the damage state of the cohesive zone is predicted to $\delta^{\text{tr}} = |\mathbf{u}_e(\mathbf{x}_d)| = \sqrt{\mathbf{u}_e(\mathbf{x}_d) \cdot \mathbf{u}_e(\mathbf{x}_d)}$. Based on that prediction the total traction, i.e., cohesive and penalty contributions reads

$$\mathbf{T} = \frac{\partial \psi}{\partial \mathbf{u}_e} = \underbrace{c \mathbf{u}_e}_{\text{cohesive}} + \underbrace{k \langle u_n \rangle \mathbf{n}}_{\text{penalty}}, \quad (9)$$

where the cohesive stiffness is defined by

$$c = \begin{cases} c_n & \forall \delta^{\text{tr}} < \delta_n \text{ (Elastic)}, \\ t_0 \exp[-a(\delta^{\text{tr}})^b] / \delta^{\text{tr}} & \forall \delta^{\text{tr}} \geq \delta_n \text{ (Damage)}. \end{cases} \quad (10)$$

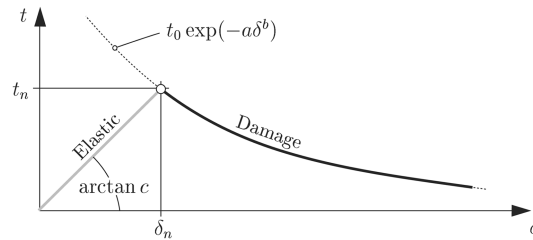


Fig. 1 Elastic and damage loading branches of the cohesive law at a state of damage δ_n

The associate total stiffness measures, i.e., cohesive and penalty contributions are given to

$$\mathbf{C}_{\mathbf{u}_e} = \frac{\partial \mathbf{T}}{\partial \mathbf{u}_e} = \underbrace{c\mathbf{I} - \gamma \mathbf{u}_e \otimes \mathbf{u}_e}_{\text{cohesive}} + \underbrace{\langle u_n \rangle \frac{k}{u_n} \mathbf{n} \otimes \mathbf{n}}_{\text{penalty}}, \quad (11)$$

$$\mathbf{C}_{\mathbf{n}} = \frac{\partial \mathbf{T}}{\partial \mathbf{n}} = \underbrace{\mathbf{0}}_{\text{cohesive}} + \underbrace{\langle u_n \rangle k (u_n^{-1} \mathbf{n} \otimes \mathbf{u}_e + \mathbf{I})}_{\text{penalty}}, \quad (12)$$

where

$$\gamma = \begin{cases} 0 & \forall \delta^{\text{tr}} < \delta_n \text{ (Elastic)}, \\ c[ab(\delta^{\text{tr}})^{b-2} + (\delta^{\text{tr}})^{-2}] & \forall \delta^{\text{tr}} \geq \delta_n \text{ (Damage)}. \end{cases} \quad (13)$$

denotes the damage softening parameter of the cohesive zone. A summary of the required expressions for a finite element implementation of the discrete material model is given in Table 1. Note that Eqs. (9)-(13) are applicable if $\delta > 0$, however, according to Eq. (8)₃ the cohesive stiffness c becomes infinite for the undamaged cohesive zone, i.e., $\delta = 0$. In order to tackle with that, a ‘quasi-rigid’ cohesive zone is utilized, where its initial (elastic) stiffness is defined by $1/\varepsilon$, where ε is machine-dependent small number. In addition, this approach guarantees compatibility of the stress field of the bulk material and the traction field of the cohesive zone under general 3D circumstances (Gasser and Holzapfel 2005). It is worth noting that a high initial stiffness $1/\varepsilon$ does not effect the condition of the global stiffness matrix, since the present approach deals with

Table 1 Implementation guide for the proposed cohesive material model with penalty constraint against penetration

-
- (1) Assume \mathbf{u}_e and \mathbf{n} of the current iteration step and δ_n of the last solution step to be given.
 - (2) Compute $\delta^{\text{tr}} = \sqrt{\mathbf{u}_e(\mathbf{x}_d) \cdot \mathbf{u}_e(\mathbf{x}_d)}$
 - (3) Perturb predicted damage parameter $\delta^{\text{tr}} = \text{MAX}(\delta^{\text{tr}}, t_0\varepsilon)$
 - (4) Define cohesive stiffness and damage softening parameter γ
 - IF ($\delta^{\text{tr}} < \delta_n$) THEN
 - $c = t_0 \exp(-a \delta_n^b) / \delta_n$, $\gamma = 0$
 - ELSE
 - $c = t_0 \exp[-a(\delta^{\text{tr}})^b] / \delta^{\text{tr}}$, $\gamma = c[ab(\delta^{\text{tr}})^{b-2} + (\delta^{\text{tr}})^{-2}]$.
 - ENDIF
 - (5) Compute cohesive traction and stiffness
 - $\mathbf{T}^{\text{coh}} = c\mathbf{u}_e$, $\mathbf{C}_{\mathbf{u}_e}^{\text{coh}} = c\mathbf{I} - \gamma \mathbf{u}_e \otimes \mathbf{u}_e$, $\mathbf{C}_{\mathbf{n}}^{\text{coh}} = 0$
 - (6) Compute penetration $u_n = \mathbf{u}_e \cdot \mathbf{n}$ and add penalty contributions
 - IF ($u_n < 0$) THEN
 - $\mathbf{T} = \mathbf{T}^{\text{coh}}$, $\mathbf{C}_{\mathbf{u}_e} = \mathbf{C}_{\mathbf{u}_e}^{\text{coh}}$, $\mathbf{C}_{\mathbf{n}} = \mathbf{C}_{\mathbf{n}}^{\text{coh}}$.
 - ELSE
 - $\mathbf{T} = \mathbf{T}^{\text{coh}} + k u_n \mathbf{n}$, $\mathbf{C}_{\mathbf{u}_e} = \mathbf{C}_{\mathbf{u}_e}^{\text{coh}} + k \mathbf{n} \otimes \mathbf{n}$, $\mathbf{C}_{\mathbf{n}} = \mathbf{C}_{\mathbf{n}}^{\text{coh}} + k \mathbf{n} \otimes \mathbf{u}_e + u_n \mathbf{I}$.
 - ENDIFIF
 - (7) Update damage parameter if global iteration has converged
 - $\delta_n \leftarrow \text{MAX}(\delta^{\text{tr}}, \delta_n)$
-

embedded discontinuities.

2.3. Crack-tracking algorithm

A critical task to employ PUFEM is the geometrical representation of the crack surface and tracking its propagation. Especially for 3D, the development of crack-tracking algorithms is an active research area in computational mechanics. Crack-tracking schemas can be classified in *local*, *global* and *partial domain* algorithms. Local algorithms (Moës, *et al.* 2002) propagate the crack on the basis of the local (stress) situation at the crack tip, while global algorithms (Oliver, *et al.* 2004) integrate information of the whole BVP. By contrast, the partial domain algorithm (Feist and Hofstetter 2007) requires information only from parts of the BVP.

The crack-tracking algorithm based on the level set method (LSM) (Osher and Sethina 1988), is a popular local algorithms and uses signed distance functions to describe discontinuities (Stolarska, *et al.* 2001, Moës, *et al.* 2002). For the 3D case, two advance vectors, which are computed on the basis of the failure criterion, determine (locally) the advance of the crack. The values of the signed distance functions are stored at element nodes, which defines the strong discontinuity for the underlying FEM. On the other hand, a global tracking algorithm, to capture the crack path has been introduced in Oliver, Huespe, Samaniego and Chaves (2002), Oliver, *et al.* (2004). The authors propose the formulation of a linear anisotropic heat-conduction-like problem and its solution (for example using the FEM) provides all information to describe the discontinuity at the element level. Note that all topological issues are addressed by the heat-conduction-like problem, however, it needs to be solved at least after each mechanical load step, and hence, this approach is associated with computational effort. In order to avoid that, the partial domain algorithm (Feist and Hofstetter 2007) processes information within the domain actually or potentially affected by the current crack.

Herein, the recently proposed two step predictor-corrector schema (Gasser and Holzapfel 2005) is applied, which is briefly summarized. It is assumed that the failure criterion of the k -th finite element (which is located at the crack tip) is met and the associated discontinuity needs to be appended to the existing crack. The orientation of the discontinuity is defined by the failure criterion and the existing crack defines its location in space, such that a *Runge Kutter*-like problem exists. However, the straight forward application of the non-local *Rankine* criterion in a 3D setting may cause the development of a geometrically incompatible crack surface, e.g., with non-physical bifurcations. In order to circumvent these topological difficulties, a two step predictor-corrector schema is proposed, where the predictor and the corrector steps are based on the non-local *Rankine* criterion and a surface smoothing strategy, respectively (Gasser and Holzapfel 2006). In particular, the corrector step draws in non-local information of the existing crack in order to compute a ‘smooth’³ 3D crack surface. This is realized by fitting a polynomial surface $Z(X, Y)$ locally to the predicted crack surface, i.e., the crack surface defined by the predictor step. To this end n_R^* points on the crack surface (located in the vicinity Ω_0^* of the k -th finite element) are considered and the coefficients of the polynomial surface are defined by minimizing the least-square problem

$$\Phi = \sum_{i=1}^{n_R^*} (Z_i - Z(X_i, Y_i))^2 \rightarrow \text{MIN}, \quad (14)$$

³It need to be emphasized that the proposed geometrical representation of the crack leads to a C^{-1} continuous surface and ‘smooth’ has no mathematical meaning.

where X_i, Y_i, Z_i denote the components of the considered points on the crack surface. Here, Ω_0^* is assumed to be a sphere with radius R^* .

Subsequently, the orientation of the discontinuity \mathbf{N} in the k -th finite element is adapted (corrected) to the normal onto the polynomial surface $Z(X, Y)$ (Gasser and Holzapfel 2006). This leads to a ‘smooth’ prediction of the crack surface and effectively circumvents topological difficulties, which might arise from the predictor step.

The proposed crack-tracking algorithm has been implemented in a separate user macro and linked to the multi-purpose finite element analysis program FEAP (Taylor 2000). The macro is executed after each mechanical loading step and the user has to specify R^* and the degree of the polynomial surface; the current implementation supports linear and quadratic surfaces as well.

3. The PCT3D test

The introduced computational concept, i.e., the PUFEM combined with the predictor-corrector scheme (Gasser and Holzapfel 2006) to track non-planar 3D cracks, has been employed to predict concrete failure during the PCT3D test. The computations are performed using the multi-purpose finite element analysis program FEAP (Taylor 2000) running on a PENTIUM 4 PC with 1.0 Gb RAM. In this section a detailed description of the numerical model of the PCT3D test is given and the applied solution strategy are discussed briefly. Finally, the predicted numerical results are presented and compared to experimental data, which is presented in the companion paper (Feist and Hofstetter 2007).

3.1. Modeling details

Geometry, boundary conditions and applied loading of the PCT3D test are sketched in Fig. 2 and detailed information is given in Feist and Hofstetter (2007). The applied unstructured finite element mesh is generated by the software-package NETGEN (Schöberl 2002) and the mesh is *a priori* refined in the region where failure was expected according to the experimental work (Feist and Hofstetter 2007). For the present computation, the finite element discretization used constant strain tetrahedral elements and the applied material parameters are listed in Table 2. Here the elastic parameters κ, μ represent the mean values from concrete tensile tests (Feist and Hofstetter 2007), while the cohesive strength t_0 are estimated from the concrete’s characteristic compressive strength, as discussed in Feist and Hofstetter (2007). The shape of the cohesive law is determined by a, b , which are determined from least square optimization (Gasser and Holzapfel 2005) of data based on tensile tests published in Reinhardt, *et al.* (1986). According to the applied cohesive parameters the mode I fracture energy of $\mathcal{G}_f^I = 0.106 \text{ Nmm}^{-1}$ (Gasser and Holzapfel 2005) describes the concrete cracking, which is higher than the values given in Feist and Hofstetter (2007).

Displacement controlled arc-length method (Batoz and Dhatt 1979) is applied to control the computation, where the increment of the *CMOD* defines the constraint of the continuation method. *CMOD* is defined as the relative displacement between the points *A* and *B* along the axis of the beam, see Fig. 2, and has also been used to control the load in the experiment during the softening branch (Feist and Hofstetter 2007).

In order to define the failure criterion of the i -th finite element according to Eq. (5), the Cauchy stress is averaged within the (referential) sphere $\bar{\Omega}_0(\mathbf{X}_c)$, where \mathbf{X}_c denotes the referential center of the i -th finite element. For the present computation the radius of the sphere is taken to be $R =$

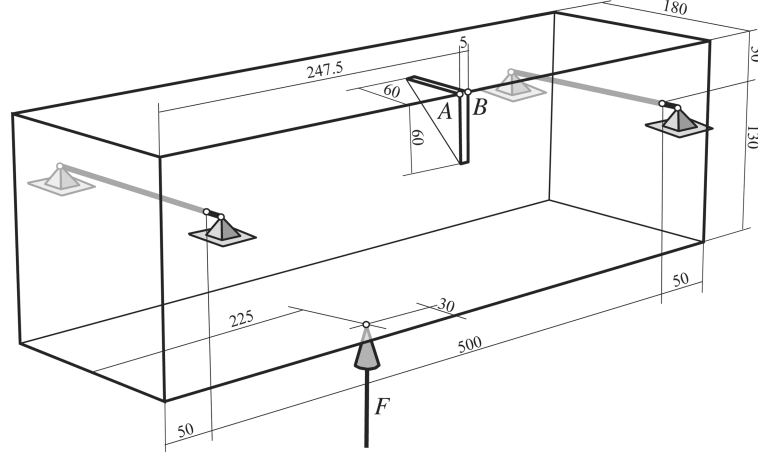


Fig. 2 Geometry, boundary conditions and loading conditions of the PCT3D test (Feist and Hofstetter 2007). *CMOD* is defined as the relative displacement of *A* and *B* along the axes of the beam. (All dimensions are in millimeter).

Table 2 Bulk and cohesive material parameters applied

| | | |
|---------------------------------|-------------------------|------------------------------|
| Bulk modulus κ | $20.23 \cdot 10^3$ MPa | } Bulk material response |
| Shear modulus μ | $15.63 \cdot 10^3$ MPa | |
| Cohesive tensile strength t_0 | 3.05 MPa | } Cohesive material response |
| Cohesive parameter a | 11.32 mm^{-1} | |
| Cohesive parameter b | 0.674 | |

$3.0\sqrt[3]{V_i}$, where V_i denotes the referential element volume. The average Cauchy stress is computed according to $\bar{\sigma} = (\sum_j \sigma_j^e V_j^e) / \sum_j V_j^e$, where the index j runs over all finite elements with (referential) centers in $\Omega_0(\mathbf{X}_c)$. Here, σ_j^e and V_j^e denotes the Cauchy stress of the j -th finite element and its referential volume, respectively. The orientation \mathbf{N} of the discontinuity to be embedded in the i -th finite element is characterized by the non-local *Rankine* criterion and subsequently modified according to the proposed smoothing technique (corrector step), where a linear polynomial surface $Z(X, Y)$ has been applied. The corrector step considers points on the referential crack surface within the sphere $\Omega^*(\mathbf{X}_c)$ of radius $R^* = 2.0\sqrt[3]{V_i}$ and center \mathbf{X}_c .

3.2. Predicted results

The computation used 232 load steps to reach $CMOD=0.8$ mm, and within each load step 5 iterations are performed to propagate the crack. Here the failure criterion is checked, and, if required, the crack is propagated, i.e., further discontinuities are embedded. If the crack propagated during the nested loop the global system needed to be solved again. A *symmetric* direct solver based on triangular decomposition of the system stiffness matrix has been applied. It needs to be emphasized that although the system stiffness matrix is not symmetric, as mentioned in Section 2.2 and discussed in Gasser and Holzapfel (2003b), the problem exhibited (about) quadratic convergence at the solution point. Obviously, non-symmetric contributions of the system stiffness matrix are negligible for the

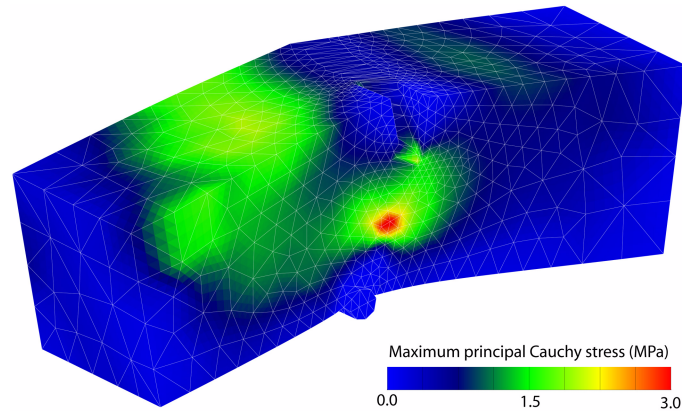


Fig. 3 Maximum principal Cauchy stress on top of the current configuration at the opening displacement $CMOD=0.07$ mm (displacements are scaled by a factor 500).

present problem, which might indicate that the constraint against penetration remains inactive during the computation.

3.2.1. Stress field

Fig. 3 shows the deformed configurations (displacements are scaled by a factor 500) and the maximum principal Cauchy stress at the opening displacement $CMOD=0.07$ mm. It indicates the evolution of a 3D crack and illustrates stress concentrations at the crack-tip, however, the stresses are bounded according to the underlying cohesive tensile strength t_0 , which is in clear contradiction to stress singularities at sharp crack-tips. Hence, a mesh refinement at the crack-tip would not essentially change the computed results.

3.2.2. Crack formation

Fig. 4 shows the predicted crack with respect to the reference configuration at opening displacements $CMOD=0.02, 0.06, 0.8$ mm. The figure nicely illustrates, that the 3D stress state of the PCT3D test causes a double curved crack, similar to experimental observations, see, Feist and Hofstetter (2007). In order to discuss that in more details, the computed crack formations at the front, rear and back faces are compared to experimental data in Fig. 5. Here the dark line and the four gray lines denote the computed and the experimental results, respectively. A comparison with respect to the bottom face is skipped herein, because the computed crack at $CMOD=0.8$ mm has not separated the specimen completely, i.e., the crack reaches only partly the bottom face. Fig. 5 illustrates that the computed crack correlates nicely with the experimentally observed fracture formations. However, the experimental cracks have a higher curvature at the front face and the crack orientation at the beginning differs significantly at the front and top faces as well.

For the present computation, the crack has been initialized at the corner of the notch at the top face and its propagation is defined by the crack-tracking algorithm. However, it can be seen in Fig. 4 that the predicted crack does not follow the notch completely, but develops partly beside it. A possible explanation for that can be found in the relatively coarse finite element mesh at the notch and probably mesh refinement might force the crack to follow the edge of the notch.

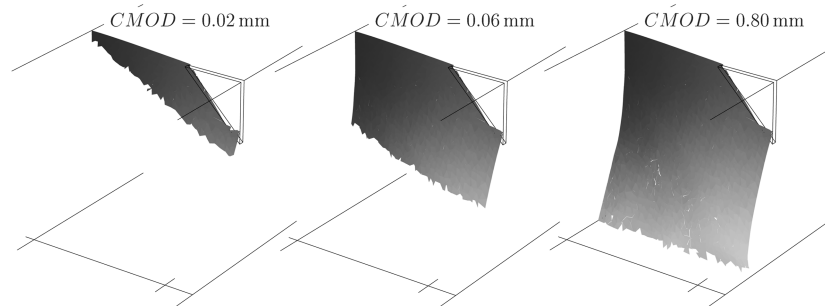


Fig. 4 Evolution of double curved crack with respect to the reference configuration. Three particular opening displacements are considered, i.e., $CMOD=0.02, 0.06, 0.80$ mm.

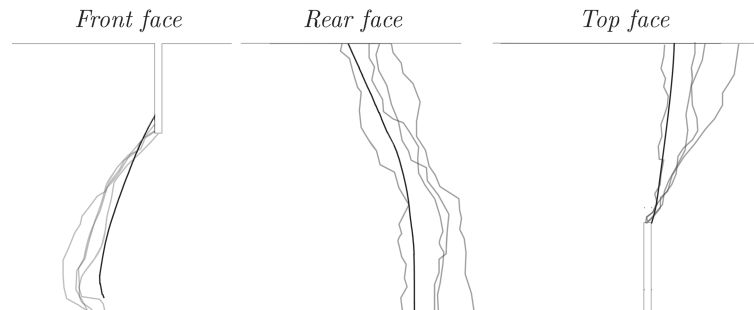


Fig. 5 Numerically predicted and experimentally observed crack formation at the front, rear and top faces. The dark solid line denotes the computed result and gray lines are experimental observed cracks of 4 PCT3D tests (Feist and Hofstetter, submitted).

3.2.3. Load-CMOD response

A comparison between the computed and the experimentally measured load F with respect to $CMOD$ is presented in Fig. 6, where experimental data (according to 4 PCT3D tests (Feist and Hofstetter 2007)) and the results of the present numerical analysis are shown by the grey and black solid lines, respectively. While the computation captures the softening region nicely, an overestimation of the limit load, compared to the average of the experimental data, is predicted. However, the load- $CMOD$ response of one individual test (denoted by PCT3D/1 in Feist and Hofstetter (2007)) is closely captured by the numerical model, and interestingly enough, even the crack formation of this individual test fits best.

It is worth noting that a similar overestimation of the limit load has also been reported for several numerical studies in concrete mechanics, see amongst many others, e.g., for the *Nooru-Mohammed* test (de Borst 1997, Pivonka, *et al.* 2004, Gasser and Holzapfel 2006). Note that the applied numerical approach is free of *stress-locking*, and hence, the underlying cohesive law might be responsible for the overestimation of the limit load. It is possible that other than mode I properties define the cohesive properties at the limit load condition. At $CMOD > 0.6$ mm the computed load has the tendency to increase, which is non-physical and can be explained by the applied failure criterion in combination with the coarse finite element mesh. During the end of the crack propagation the remaining ‘non-cracked’ concrete is exposed to bending with the associated high stress gradient. This situation together with the coarse mesh (defining a large averaging volume $\Omega_0(\mathbf{X})$) might require an increasing load F in order to activate the non-local *Rankine* criterion.

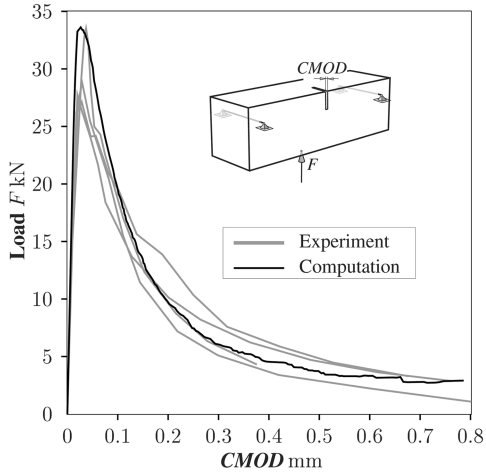


Fig. 6 Comparison of the load F - $CMOD$ response for the PCT3D test. The black line denotes results from the present computation, and the grey lines represent experimental data of 4 PCT3D tests (Feist and Hofstetter 2007).

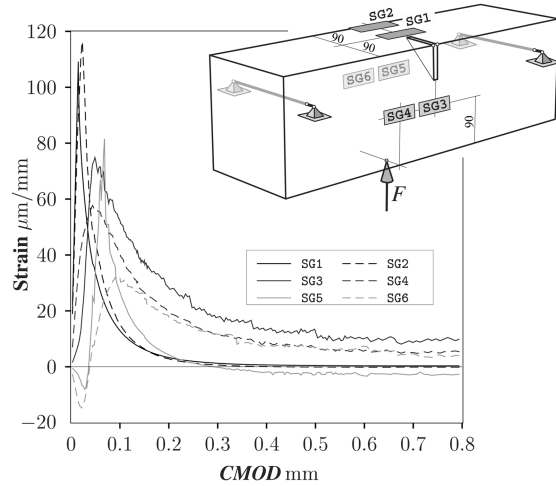


Fig. 7 Predicted strain at locations of the strain gauges SG1-SG6 in Feist and Hofstetter (2007). The results represent the strain in a fiber with referential direction along the beam's axis.

3.2.4. Strain field

The strains measured by the strain gauges SG1-SG6 in Feist and Hofstetter (2007) nicely illustrates the 3D nature of the PCT3D test, see the discussion in Feist and Hofstetter (2007). The associated predicted strains at locations denoted by SG1-SG6 are shown in Fig. 7. In particular, the evolution of the strain in a fiber with referential direction along the beam's axis are plotted. A comparison of Fig. 7 with the data given in Feist and Hofstetter (2007) indicates qualitative agreement with the associated experimental study, however, significant quantitative mismatch is present.

4. Summary and conclusions

The discrete crack-concept is applied to model tensile-dominated failure during the PCT3D test of plain concrete. Hence, irreversible processes of internal damage are assumed to be localized at zones of small volume, which are mechanically characterized by a cohesive constitutive law. The strong discontinuity approach is applied and a variationally consistent PUFEM implementation is followed. The onset of concrete fracture is determined by a non-local *Rankine* criterion and a predictor-corrector schema is applied to track the crack path. This approach effectively avoids arising geometrical difficulties and allows to handle arbitrary shaped non-interacting 3D cracks. The proposed concept led to a robust numerical description of concrete cracking during the PCT3D test and the computational predictions are compared to experimental findings. In particular, the load- $CMOD$ response, the crack formation and the strain field are compared to experimental data of the PCT3D test. Although the employed constitutive models, i.e., neoHookean model for the bulk material and a three-parameter model for the cohesive zone, are very simple, good agreement between computation and the experiment are found. However, some overestimation of the predicted peak-load and quantitative disagreement of the predicted strain field has been observed. Apart from that, the softening branch, i.e., the decay of the

load with respect to *CMOD* is captured nicely by the proposed model. In addition, the comparison of the predicted 3D crack with the experimental formations showed good agreement.

Constitutive relations are fundamental to the solution of problems in continuum mechanics, e.g., to investigate concrete cracking. The developed numerical concept provides a clear interface for constitutive models, and hence, it allows to implement more complex cohesive models for concrete in order to investigate their impact on concrete failure. Constitutive models for concrete cracking can be investigated under 3D loading conditions, which is of significant scientific interests to interpret results from 3D experiments in order to progress in that important field of solid mechanics.

References

- Batoz, J. and Dhatt, G. (1979), "Incremental displacement algorithms for nonlinear problems", *Int. J. Numer. Meth. Eng.*, **14**, 1262-1267.
- Bažant, Z.P. (2002), "Concrete fracture models: Testing and practice", *Eng. Fract. Mech.*, **69**, 165-205.
- Bažant, Z.P. and Pijaudier-Cabot, G. (1988), "Nonlocal continuum damage, localization instability and convergence", *J. Appl. Mech.*, **55**, 287-293.
- Bigoni, D. and Zaccaria, D. (1994), "On the eigenvalues of the acoustic tensor in elastoplasticity", *Eur. J. Mech. A/Solids*, **13**, 621-638.
- Brokenshire, D.R. (1996), Torsional fracture tests, PhD thesis, Cardiff University, U.K.
- Coleman, B.D. and Noll, W. (1963), "The thermodynamics of elastic materials with heat conduction and viscosity", *Arch. Rat. Mech. Anal.*, **13**, 167-178.
- Feist, C. and Hofstetter, G. (2006), "An embedded strong discontinuity model for cracking of plain concrete", *Comput. Meth. Appl. Mech. Eng.*, **195**(52), 7115-7138.
- Feist, C. and Hofstetter, G. (2007), "Validation of 3d crack propagation in plain concrete Part I: Experimental investigation -the PCT3D test", *Comput. Concrete.*, **4**(1), 49-66.
- Feist, C., W. Kerber, H. and Lehar, G.H. (2004), "A comparative study of numerical models for concrete cracking", in *Proc. of European Congress on Computational Methods in Applied Sciences and Engineering, ECCOMAS, Barcelona*, P. Neittaanmki, T. Rossi, S. Korotov, E. Onate, J. Periaux, D. Knrzer (Eds).
- Gasser, T.C. and Holzapfel, G.A. (2003a), "Geometrically non-linear and consistently linearized embedded strong discontinuity models for 3D problems with an application to the dissection analysis of soft biological tissues", *Comput. Meth. Appl. Mech. Eng.*, **192**, 5059-5098.
- Gasser, T.C. and Holzapfel, G.A. (2003b), "Necking phenomena of a ber-reinforced bar modeled by multisurface plasticity", in C. Miehe, ed., *IUTAM Symposium on Computational Mechanics of Solid Materials at Large Strains, Proceedings of the IUTAM Symposium held in Stuttgart, Germany, 20-24 August 2001*, Kluwer Academic Publishers, Dordrecht, pp. 211-220.
- Gasser, T. and Holzapfel, G. (2005), "Modeling 3D crack propagation in unreinforced concrete using PUFEM", *Comput. Meth. Appl. Mech. Eng.*, **194**, 2859-2896.
- Gasser, T. and Holzapfel, G. (2006), "3D crack propagation in unreinforced concrete. A new smooth algorithm for tracking 3D crack surfaces", *Comput. Meth. Appl. Mech. Eng.*, **195**, 5198-5219.
- Holzapfel, G.A. (2000), *Nonlinear Solid Mechanics. A Continuum Approach for Engineering*, John Wiley & Sons, Chichester.
- Jefferson, A.D. (2003a), "CRAFT -A plastic-damage-contact model for concrete. I. Model theory and thermodynamic considerations", *Int. J. Solids Struct.*, **40**, 5973-5999.
- Jefferson, A.D. (2003b), "CRAFT -A plastic-damage-co,ntact model for concrete. II. Model implementation with implicit return-mapping algorithm and consistent tangent matrix", *Int. J. Solid Struct.* **40**, 6001-6022.
- Jirásek, M. (2000), "Comparative study on finite elements with embedded discontinuities", *Comput. Meth. Appl. Mech. Eng.*, **188**, 307-330.
- Jirásek, M. and Belytschko, T. (2002), "Computational resolution of strong discontinuities", in *Proc. World Congress on Computational Mechanics, WCCM V*, H. Mang, F. Rammerstorfer and J. Eberhardsteiner (Eds), Vienna University of Technology, Austria.
- Kesler, C.E., Naus, D.J. and Lott, J.L. (1972), "Fracture mechanics -its applicability to concrete", in *Proceedings of the International Conference on the Mechanical Behavior of Materials*, The Society of Material Sciences,

- Kyoto 1971, pp. 113-124.
- Mandel, J. (1966), "Conditions de stabilité et postulat de Drucker", in J. Kravtchenko and P.M. Sirieys, eds, *Rheology and Soil Mechanics*, Berlin, Germany, pp. 58-68.
- de Borst, R. (1997), "Some recent developments in computational modelling of concrete fracture", *Int. J. Fracture*, **86**, 5-36.
- de Borst, R. (2001), "Some recent issues in computational failure mechanics", *Int. J. Numer. Meth. Eng.*, **52**, 63-95.
- Melenk, J. and Babuška, I. (1996), "The partition of unity finite element method: Basic theory and applications", *Comput. Meth. Appl. Mech. Eng.*, **139**, 289-314.
- Moës, N., Gravouil, A. and Belytschko, T. (2002), "Non-planar 3D crack growth by the extended finite element and level sets - Part I: Mechanical model", *Int. J. Numer. Meth. Eng.*, **53**, 2549-2568.
- Needleman, A. (1987), "A continuum model for void nucleation by inclusion debonding", *J. Appl. Mech.*, **54**, 525-531.
- Needleman, A. (1990), "An analysis of decohesion along an imperfect interface", *Int. J. Fracture*, **42**, 21-40.
- Ogden, R.W. (1997), *Non-linear Elastic Deformations*, Dover, New York.
- Oliver, J. (2000), "On the discrete constitutive models induced by strong discontinuity kinematics and continuum constitutive equations", *Int. J. Solids Struct.* **37**, 7207-7229.
- Oliver, J., Huespe, A.E., Samaniego, E. and Chaves, E.W.V. (2002), "On strategies for tracking strong discontinuities in computational failure mechanics", in H.A. Mang, F.G. Rammerstorfer and J. Eberhardsteiner, eds, *Proceedings of the Fifth World Congress on Computational Mechanics (WCCM V)*, Vienna University of Technology, Vienna, Austria.
- Oliver, J., Huespe, A.E., Samaniego, E. and Chaves, E.W.V. (2004), "Continuum approach to the numerical simulation of material failure in concrete", *Int. J. Numer. Anal. Meth. Geomech.*, **28**, 609-632.
- Oliver, J., Huespe, A., Pulido, M. and Chaves, E. (2002), "From continuum mechanics to fracture mechanics: The strong discontinuity approach", *Eng. Fract. Mech.*, **69**, 113-136.
- Ortiz, M. and Pandolfi, A. (1999), "Finite-deformation irreversible cohesive elements for three-dimensional crack-propagation analysis", *Int. J. Numer. Meth. Eng.*, **44**, 1267-1282.
- Osher, S. and Sethian, J.A. (1988), "Fronts propagating with curvature depending speed: Algorithms based on hamilton-jacobi formulations", *J. Comput. Phys.*, **79**, 12-49.
- Pivonka, P., Ožbolt, J., Lackner, R. and Mang, H.A. (2004), "Comparative studies of 3d constitutive models for concrete: application to mixed-mode fracture", *Int. J. Numer. Meth. Eng.*, **60**, 549-570.
- Reinhardt, H.W., Cornelissen, H.A.W. and Hordijk, D.A. (1986), "Tensile tests and failure analysis of concrete", *J. Struct. Eng.-ASCE*, **112**, 2462-2477.
- Rudnicki, J.W. and Rice, J.R. (1975), "Conditions for the localization of deformation in pressure-sensitive dilatant materials", *J. Mech. Phys. Solids*, **23**, 371-394.
- Schöberl, J. (2002), *NETGEN - A 3D tetrahedral mesh generator - Version 4.2*, University Linz, Austria.
- Simone, A., Askes, H. and Sluys, L. (2004), "Incorrect initiation and propagation of failure in non-local and gradient-enhanced media", *Int. J. Solids Struct.*, **41**, 351-363.
- Spencer, A.J.M. (1984), "Constitutive theory for strongly anisotropic solids", in A.J.M. Spencer, ed., *Continuum Theory of the Mechanics of Fibre-Reinforced Composites*, T. Christian Gasser Springer-Verlag, Wien, pp. 1-32. *CISM Courses and Lectures No. 282*, International Centre for Mechanical Sciences.
- Stolarska, M., Chopp, D.L., Moës, N. and Belytschko, T. (2001), "Modelling crack growth by level sets in the extended finite element method", *Int. J. Numer. Meth. Eng.*, **51**, 943-960.
- Taylor, R.L. (2000), *FEAP - A Finite Element Analysis Program - Version 7.3*, University of California at Berkeley.
- Tvergaard, V. and Hutchinson, J.W. (1992), "The relation between crack growth resistance and fracture process parameters in elastic-plastic solids", *J. Mech. Phys. Solids*, **40**, 1377-1397.
- Varias, A.G., O'Dowd, N.P., Asaro, R.J. and Shih, C.F. (1990), "Failure of bimaterial interfaces", *Materials Sci. Eng., A* **126**, 65-93.
- Wells, G.N., de Borst, R. and Sluys, L.J. (2002), "A consistent geometrically non-linear approach for delamination", *Int. J. Numer. Meth. Eng.*, **54**, 1333-1355.
- Wells, G.N. and Sluys, L.J. (2001), "Three-dimensional embedded discontinuity model for brittle fracture", *Int. J. Solids Struct.*, **38**, 897-913.
- Wriggers, P. (2002), *Computational Contact Mechanics*, John Wiley & Sons, Chichester.